Soft Matter

PAPER

Cite this: *Soft Matter*, 2022, **18**, 1554

Gelation under stress: impact of shear flow on the formation and mechanical properties of methylcellulose hydrogels†

Arif Z. Nelson,[a] Yilin Wang,[a] Yushi Wang,[a] Anthony S. Margotta,[a] Robert L. Sammler,[b] Aslin Izmitli,[c] Joshua S. Katz,[d] Jaime Curtis-Fisk,[b] Yongfu Li[e] and Randy H. Ewoldt*[a]

Received 2nd December 2021,
Accepted 20th January 2022

DOI: 10.1039/d1sm01711j

rsc.li/soft-matter-journal

We demonstrate that small unidirectional applied-stresses during temperature-induced gelation dramatically change the gel temperature and the resulting mechanical properties and structure of aqueous methylcellulose (MC), a material that forms a brittle gel with a fibrillar microstructure at elevated temperatures. Applied stress makes gelation more difficult, evidenced by an increased gelation temperature, and weakens mechanical properties of the hot gel, evidenced by a decreased elastic modulus and decreased apparent failure stress. In extreme cases, formation of a fully percolated polymer network is inhibited and a soft granular yield-stress fluid is formed. We quantify the effects of the applied stress using a filament-based mechanical model to relate the measured properties to the structural features of the fibril network. The dramatic changes in the gel temperature and hot gel properties give more design freedom to processing-dependent rheology, but could be detrimental to coating applications where gravitational stress during gelation is unavoidable.

1. Introduction

The industrial, consumer, and scholarly importance of methylcellulose (MC) is immense. The hydrophobic modification of cellulose—the most abundant material in nature—yields MC which has been utilized to considerable effect in pharmaceuticals research,[1–4] food products,[5–7] building materials,[8,9] packaging films,[10,11] solar cells,[12] fuel cells,[13,14] nano-particle synthesis,[15,16] and research on cell culturing.[17–19] The most immediately intriguing aspect of aqueous MC is its uncommon ability to form a turbid, thermoreversible gel at elevated temperatures as shown in Fig. 1a. There has been much progress made in studying the structure and rheological properties of MC solution and gel,[20–32] as well as the dependence of gelation on degree of substitution,[33] concentration,[21,34] ion concentration,[35] and heating rate.[26]

Almost the entire rich body of work that exists on gelling aqueous MC focuses on gels that form in a completely- or quasi-undisturbed state, such as oscillatory shear at small forcing amplitude. Although this characterization method is not strictly quiescent, here we refer to quasi-undisturbed oscillatory deformation (with zero time-averaged forcing) as "quiescent" to contrast with unidirectional applied stress which we refer to as "dynamic". Under quiescent conditions, MC has been observed to form a fibrillar gel network.[27,28] This network results from a conformational change of MC polymers in solution from coils to rings and self-assembly into fibrils.[36,37] The material shown in Fig. 1a was gelled in this quiescent

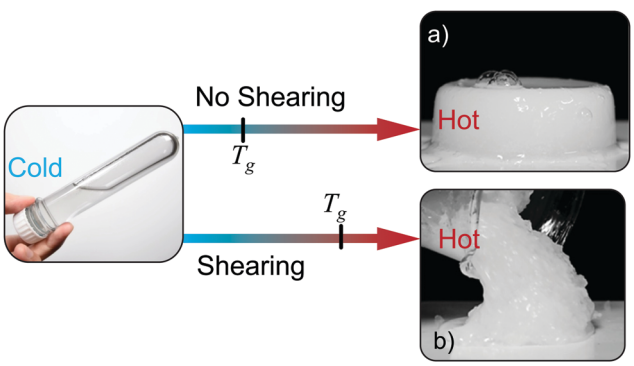

Fig. 1 Images of gels resulting from heating aqueous MC solutions. (a) Gel formed while undisturbed during heating. (b) Gel formed while exposed to a constant rotational velocity from an overhead stirrer.

[a] *Department of Mechanical Science and Engineering, University of Illinois at Urbana-Champaign, Urbana, IL 61801, USA. E-mail: ewoldt@illinois.edu*
[b] *Formulation, Automation, and Material Science and Engineering, Corporate R&D, Dow Inc., Midland, MI 48674, USA*
[c] *Home and Personal Care TS&D, Dow Inc., Collegeville, PA 19426, USA*
[d] *Pharma Solutions R&D, International Flavors & Fragrances, Wilmington, DE 19803, USA*
[e] *Analytical Science, Corporate R&D, Dow Inc., Midland, MI 48674, USA*

† Electronic supplementary information (ESI) available. See DOI: 10.1039/d1sm01711j

manner, and the ultimate mode of failure is fracture at a critical shear stress, rather than ductile yielding and flowing. However, for many of the applications mentioned above and others, MC is not gelled in a quiescent condition but rather under dynamic conditions, such as a coating applied to a vertical surface with gravity inducing a shear stress. In this case, the properties of quiescently gelled MC studied previously may be totally unrepresentative of how the material will actually behave under finite stress conditions; under appropriate processing conditions (*e.g.* strong shear while heating), dramatically different properties result. Shown in Fig. 1b, heating while continuously mixing results in a soft granular yield-stress fluid (also known as false body) that flows at high stress and nevertheless behaves as a solid at low stress.[38] Gel point determination from shear rheology is typically performed with a small imposed stress or strain, and any effect on the gel point is assumed to be negligible.[39–42] Yet the finite stresses imposed (either oscillatory or unidirectional) during gelation[43] may affect the network formation, changing the gelling process, the corresponding gel point, and the mechanical properties of the gel formed. Therefore, the effect of dynamic conditions on gelation needs to be considered for meaningful characterization.

The importance of investigating the effect of deformation and flow conditions on structure formation has been identified for many material systems with network microstructures. Though most studies use controlled deformation rate conditions,[44–50] comparatively few investigate the effect of controlled stress[51,52] which may be more relevant to application flow conditions.[53,54] The effect of controlled shear rate conditions and inhomogeneous stresses imposed by extrusion during temperature-ramp gelation of aqueous MC was investigated by Knarr and Bayer,[55] who found that forcing a constant deformation rate will destroy the gel network that forms on heating, and cause gelation to occur at higher temperatures. However, the resulting rheological properties after gelation were not studied and a fully-formed gel under loaded conditions could not be observed due to fixed shear rate rather than fixed stress conditions. Applied unidirectional stress—rather than rate—is common in applications, such as coating applied to a vertical surface subject to gravitational loading. The effect of controlled-stress conditions is highly relevant to gelation during processes such as film formation, surface coating through impact, particle settling, and pressure-driven extrusion. In contrast to controlled shear rate conditions that have been found to always break down a network,[51] applying a moderate stress may allow the formation of a fully-percolated gel network strong enough to bear the applied load but that has properties different from the quiescently gelled material. This is because stresses could lead to a preferential orientation of the gel structure and rupture at the most tenuous connections of the network. A gelation temperature can still be defined with unidirectional controlled-stress conditions using the fundamental definition of the temperature at which the viscosity, η, diverges to infinity.

A fibrillar gel network structure has been reported for MC polymers of molecular weights 150 kg mol^{-1} and higher,[36,56] but currently the precise microstructure of the material used in our study here (M_w approximately 50 kg mol^{-1}, details given below) is still unknown. The material used in this study becomes optically turbid (Fig. 1) as temperature increases and gel forms, similar to the MC with higher molecular weights,[26] indicating the presence of large scale heterogeneities in the microstructure. The change in turbidity has been characterized in previous studies.[29] Microstructure characterization under shear flow has not been reported for this material, and is complicated due to the high temperatures involved. This could be possible with orthogonal superposition rheometry,[57] or experimental setups that combine rheometry and structure characterization (scattering[58,59] or confocal[60,61]), but this is outside the scope of the work here.

In this work, we systematically apply constant unidirectional shear stresses while heating to probe the rheology of aqueous MC in both liquid and gel states for a range of concentrations. These rheological properties are compared to those obtained from quiescent gelation using a common heating rate of 1 °C min^{-1}. We will refer to gelation under constant unidirectional non-zero shear stress as dynamic gelation, in contrast with quiescent gelation. For all applications mentioned above and others, the processing-to-property space that we generate here reveals the possible catastrophic inaccuracy in gel temperature and hot gel properties for MC gels when not taking processing/application conditions into account. The molecular features of the gel are inferred from measured gel properties by using a filament-based mechanical model[29,62,63] which we adapt to rationalize the effect of applied stresses on gelation.

2. Material and methods

2.1. Material and specimen preparation

Methylcellulose used in this study was provided by International Flavors & Fragrances under the trade name METHOCEL™ A15. The MC material was characterized by size-exclusion chromatography to obtain the absolute molecular weight distribution and differential solution viscosity by the method of Li *et al.*[64] The molecular weight distribution was unimodal with number- and weight-average molecular weights of 22 and 47 kg mol^{-1}, respectively. The differential solution viscosity data (28 °C, 0.02–0.2 wt% MC) relative to that for solvent were converted into intrinsic viscosity, $[\eta]$, (167 mL g^{-1}), which was used to compute the overlap concentration ($c^* \approx [\eta]^{-1} = 0.0059$ g mL^{-1}). The degree of methyl ether substitution (DS = 1.9 mol –OCH_3 per mole AGU) was measured by an approach reported elsewhere.[65]

Prior to use, MC was dried under vacuum at 60 °C for a minimum of 12 h. Solutions were prepared by adding MC powder to half of the required amount of deionized water at 70 °C with constant stirring for 10 min without additional heating, creating an opaque dispersion. The remaining water (~21 °C) was then added gradually over 1 min, and the solution was stirred for an additional 10 min. Then it was stirred in an ice bath for 10 min and stored at 4 °C for a minimum of 12 h to fully hydrate the polymer before use. Prior to testing, solutions were degassed to minimize bubble formation when warming.

The resulting solutions went from transparent at low concentrations to translucent at higher concentrations. The density of MC is 1.39 g mL^{-1}, and the concentration was calculated assuming volume additivity as used in other MC studies.[26,29] MC solutions were prepared over the range of 1 to 8 wt% which nominally is the range of $1.75c^*$ to $13c^*$.

2.2. Rheology

Fig. 2 schematically shows the applied thermal and stress protocols. All tests were performed on TA Instruments DHR-3 and AR-G2 rotational rheometers (combined motor/transducer instruments) using a DIN concentric cylinder cup (30.4 mm diameter) and sandblasted bob (28 mm diameter, 42 mm immersed length) geometry with Peltier temperature control. To inhibit dehydration, a thin layer of mineral oil (obtained from Sigma-Aldrich) with a density of 0.838 g mL^{-1} was floated over the surface of the MC solution. For all experiments, the sample was equilibrated at 20 °C and zero applied stress for 10 min. All experiments were repeated thrice to obtain error bars; error bars smaller than data points are not shown.

The sample was warmed from 20 to 80 °C at a rate of 1 °C min^{-1}, and different stress protocols were applied simultaneously.

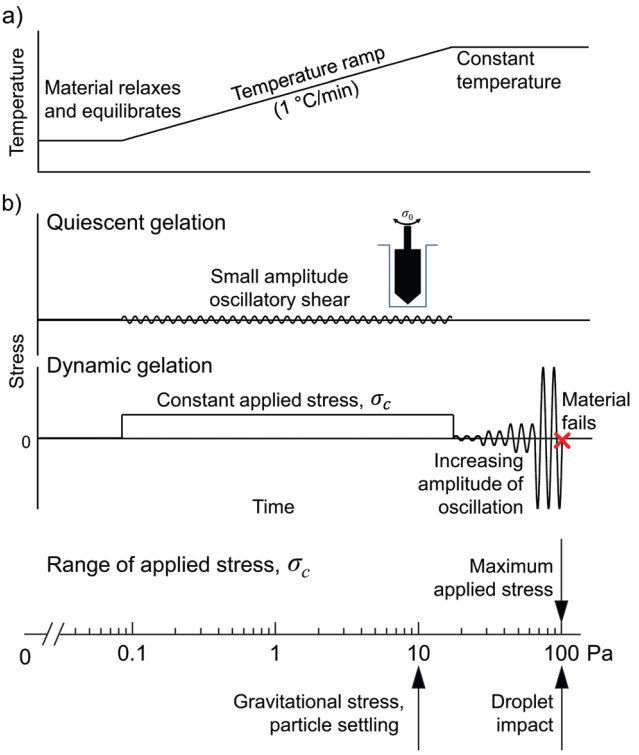

Fig. 2 Thermorheological test protocols. (a) Temperature ramp and (b) simultaneously applied stress history, two options shown: small amplitude oscillatory shear (SAOS) to probe gelation under (nearly) quiescent conditions, or a constant unidirectional stress to study dynamic gelation as a function of applied stress. After dynamic gelation, at 80 °C, an increasing oscillatory stress amplitude is applied until failure, characterizing the hot gel moduli and apparent failure stress. The axis at the bottom shows the range of shear stress applied during gelation compared to application-relevant values (calculations in Section I, ESI†). (See Video S1 for a time lapse of the dynamic gelation experiment with arrested motion due to heating and gelation, ESI.†)

For quiescent gelation, small-amplitude oscillatory shear (SAOS) measurements were performed at a frequency of 0.1 rad s^{-1} and stress amplitude of 0.1 Pa, which is within the linear regime for all the concentrations tested. This provided the elastic and viscous moduli, G' and G'', respectively, as a function of temperature. For dynamic gelation, constant unidirectional stress, σ_c, was applied and the instantaneous shear rate, $\dot{\gamma}(t)$, was measured, providing the apparent viscosity, $\eta = \sigma_c/\dot{\gamma}(t)$, as a function of temperature (see ESI† for Video S1 that demonstrates the arrested motion due to gelation at elevated temperature). The range of stress investigated here is from 0.1 to 100 Pa, as this is sufficient to inhibit gel formation for the range of concentrations studied, and more importantly, it covers several relevant application stress conditions.[53] Fig. 2b shows the applied stress range compared to benchmark values (see Section I for calculation details, ESI†). Important reference values include gravity-induced shear stress in a 1 mm thick layer on a vertical surface (10 Pa), a 1 mm particle settling (or not) due to gravity (10 Pa), and droplet impact at 0.3 m s^{-1} (100 Pa), for example in spray coating applications.

After the temperature was raised to 80 °C and the gel formed, a stress-controlled large-amplitude oscillatory shear (LAOS) was applied with increasing amplitude at a frequency of 3 rad s^{-1} until the apparent failure stress, σ_Y^*, was observed. A special case of the constant-stress gelation is $\sigma_c = 0$, to which we refer as "true quiescent" gelation (no SAOS applied during gelation). All hot gel properties (elastic modulus G' and failure stress σ_Y^*) labeled "0 Pa" are from true quiescent tests. For some high concentrations in the concentric cylinder geometry, the apparent failure stress exceeded what could be applied by the maximum instrument torque. For these materials, the hot gel properties were obtained by performing the dynamic gelation tests using a 40 mm sandblasted parallel plate on the previously specified rheometers with a Peltier flat plate and an applied mineral oil barrier. Due to maximum allowable rheometer rotation speeds, lower concentration (lower viscosity) samples were limited in the maximum stresses that could be applied during gelation.

2.3. Gel point

The gelation of MC of higher molecular weights than the one studied here has been shown to satisfy the Winter and Chambon criteria[66,67] and the frequency-independent gel temperature has been determined in a wide range of concentrations.[26] In this study, we did not determine the quiescent critical gel temperature using multiple frequencies, but pragmatically report a crossover temperature $T(G' = G'')$ at a single frequency of 0.1 rad s^{-1} for quiescently gelled samples, at which the viscoelastic storage and loss moduli are equal.[68] Although this is not a true, frequency-independent critical gel point, it is a practical reference given that we are limited to lower frequencies by instrument inertia,[69] which is a significant issue at low MC concentrations. This crossover temperature is used as a reference for comparison to the unidirectional stress dynamic gelation. The crossover temperature is plotted as the reference temperature for "0 Pa" gelation for all concentrations.

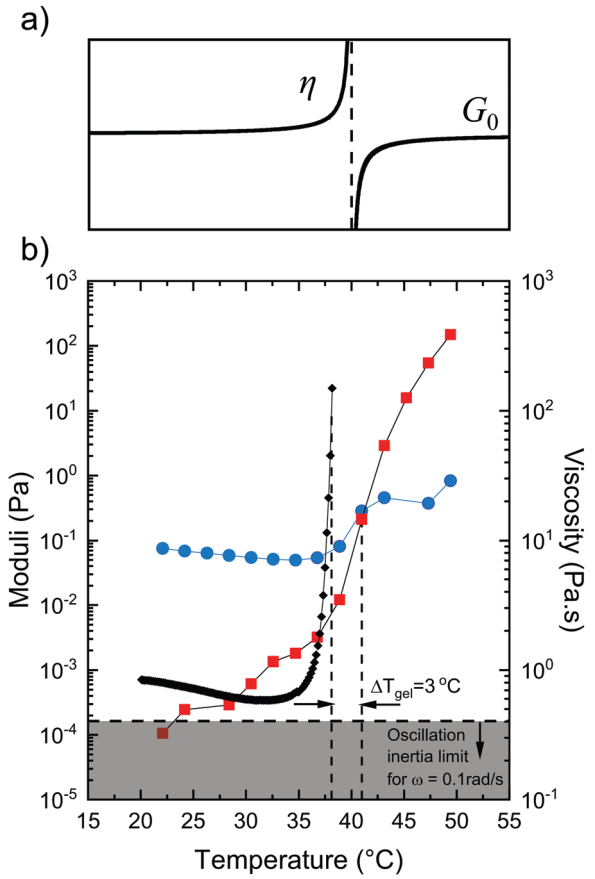

Fig. 3 Gel point from viscosity divergence. (a) Schematic of the gel point defined by diverging viscosity η and asymptotic emergence of solid elastic modulus G_0. (b) Example measurement of viscosity growth of aqueous MC (8 wt%) at 0.1 Pa applied unidirectional stress compared to SAOS measurement of G' and G'' at oscillation frequency 0.1 rad s^{-1} and stress amplitude 0.1 Pa, all while warming from 20 to 80 °C at 1 °C min^{-1}. The temperature at maximum measurable slope of η is compared to the crossover in G' and G''; the difference ΔT is an estimate of the expected variance of the methods.

For dynamic gelation tests, in which a constant unidirectional stress is applied, we use the fundamental definition of the gel temperature as the temperature at which the viscosity, η, diverges to infinity.[70] When using this definition, the ability to measure very small rates of deformation is a factor, and thus practically we determine the dynamic gel temperature using the first maximum of $\frac{d\eta}{dT}X$ when the instantaneous apparent viscosity becomes immeasurably large (solidification). A similar protocol has been used to determine the gel temperature of a triblock copolymer system, but only for stresses small enough to not significantly affect the properties of the material.[71]

Fig. 3 overlays the viscosity growth and viscoelastic moduli for the same MC concentration (8 wt%) with the same magnitude of applied stress (0.1 Pa). The dynamic gelation temperature (viscosity divergence) deviates by approximately 3 °C from the oscillatory deformation crossover temperature. We again emphasize that neither metric is the frequency-independent critical gel point because the crossover temperature may be frequency dependent and is limited by the instrument inertia effects, and the dynamic gelation temperature is the gel point under unidirectional applied stress.

3. Results and discussion

3.1. Gel point and liquid properties

Fig. 4a and b show dynamic gelation experiments for the two extreme compositions: 8 wt% and 1.04 wt%. In both cases, applied stress delays and disrupts the gelation process. In Fig. 4a, for 8 wt% MC, it is shown that $\left.\frac{d\eta}{dT}\right|_{max}$ occurs at higher temperatures with increasing applied stress, meaning that gelation occurs later, *i.e.* the material is more difficult to gel. Compared to an applied stress of 0.1 Pa, applying a stress of 100 Pa delays gelation by approximately 20 °C for these conditions of warming at 1 °C min^{-1}. This is a significant shift

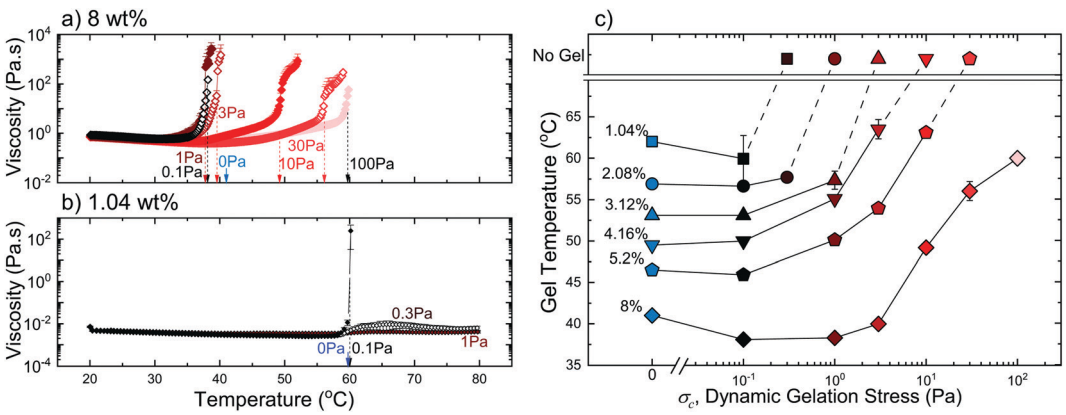

Fig. 4 Delay and disruption of gelation for aqueous MC at (a) 8 wt%, (b) 1.04 wt% and (c) all concentrations while warming from 20 to 80 °C at 1 °C min^{-1} at different unidirectional shear stress. Apparent gelation temperatures are marked with down-pointing arrows labeled with the applied shear stress. For reference, the SAOS-measured crossover temperatures at 0.1 rad s^{-1} are shown (blue arrows, labeled "0 Pa"). Full details of underlying time- and frequency-sweeps in Section II (ESI†). Color and shape of symbols for a given sample are consistent across all dynamic gelation figures.

compared to the expected variance of the different gelation methods (Fig. 3). Fig. 4b shows that at lower concentrations the gelation may be completely inhibited above a critical stress. Even at 0.3 Pa (which is very low, *cf.* Fig. 2b), the viscosity of this low concentration MC material never diverges, indicating that the imposed stress does not allow a fully-percolated gel network to form. Results for the other four concentrations are shown in Fig. S7–S10 (ESI†). At low stress, viscosity will diverge with temperature. For higher stresses the viscosity evolution is more complex, sometimes changing concavity as if gelation is interrupted, delayed, or inhibited. Materials that do not show a diverging viscosity can be considered to not gel while a sufficiently high stress is being applied. However, once the stress is removed, it is apparent from viscoelastic measurements that a soft viscoelastic solid exists (*i.e.* $G' > G''$). We interpret this structuration to be akin to rapid thixotropic recovery of a flowable yield-stress fluid rather than gelation kinetics as the gelation timescale due to a sudden temperature rise for MC gels reportedly may exceed 150 seconds depending on the concentration.[72] The amount of time between the stress removal and the oscillatory flow measurement may affect the measured properties since it gives more time for a network to form. However, here we begin oscillatory measurements immediately after the cessation of flow, and a study of the effect of network formation time is outside the scope of this work.

Fig. 4c summarizes the dynamic gel temperature results, obtained from viscosity divergence, for all studied concentrations and applied stresses. Complete data sets are reported in Section II (ESI†). The dynamic gel temperatures decrease with MC concentration at a given applied stress, σ_c, which is consistent with quiescent gelation temperature trends reported in literature.[21,26,34] Higher applied stress results in a significant increase (delay) in gel temperature for all concentrations. For all but the highest concentration, we observe a sufficiently large shear stress where dynamic gelation does not occur (labeled "No Gel" in Fig. 4c); we refer to this as the critical stress, σ_{crit}. By performing a more gradual increase in the applied stress, it would be possible to more precisely determine this critical stress to inhibit gelation if this were desired. In general, we observe that the critical stress increases with concentration as one might expect; since the macroscopic stress is determined by both the microscopic deformation of fibrils and the density of the network fibrils, at higher concentrations the applied stress to destroy the network needs to be larger for the more numerous fibrils to experience the same degree of deformation. The SAOS crossover temperatures at 1 rad s^{-1} (in blue) are shown for reference; these also decrease with concentration. At σ_c = 0.1 Pa for each concentration, the dynamic gel temperature agrees within a few degrees of the SAOS crossover temperature, as anticipated from Fig. 3.

For the highest concentration tested, 8 wt%, there is a narrow range of applied stress σ_c where the apparent gel temperature is unchanged, indicated by a plateau at low σ_c. For lower concentrations, no plateau is observed within the range of stresses tested, suggesting that the true quiescent gelation temperature may be even lower and require stresses smaller than 0.1 Pa. This is already an incredibly low stress (*cf.* Fig. 2b), revealing the need to consider the gel temperature as a function of applied stress for any rheological measurement protocol. For a truly quiescent rheological probe of gelation temperature where no additional stress or strain is imposed, it is likely that one would have to perform passive bead microrheology[73] or a similar technique.

For the MC material investigated here, we attribute the inhibition of gelation to either the destruction or prevention of fibril network connections due to flow stress, which is counteracted by the propensity to form fibrils and a percolated network at elevated temperature. When gelation is completely inhibited ('No Gel' location in Fig. 4c), it is likely that network formation is still occurring, but on length scales that do not span the full sample size until after the dynamic gelation stress is removed (and flow ceases). Evidence for this is visual (*e.g.* Fig. 1b with the soft granular yield-stress material) and with measured rheology: when the stress is removed, a soft solid forms with an apparent failure stress below the applied stress during gel formation, as discussed in the next section.

Fig. 4c can be interpreted as a regime map for dynamic gelation as a function of (T, σ_c) at a given concentration, c. For a given concentration, gelation occurs above the lines connecting the symbols, and does not occur for conditions below the lines. Of course, this regime map in Fig. 4c is only for a particular MC material and heating rate, and only for unidirectional stress. However, we anticipate that the trend of increased gel temperature and inhibited gelation under dynamic flow conditions is general to other thermally-gelling materials and heating rates, and that the effect of other dynamic conditions, such as oscillatory stress or strain rate, would disrupt the gelation similarly.

3.2. Hot gel properties

We hypothesized that gels formed under dynamic applied stress would be softer (lower storage modulus) and weaker (lower failure stress) than if formed in quiescent conditions. To assess this, hot gels were subjected to oscillatory shear stress at successively higher stress amplitudes until apparent failure was observed (see the protocol schematic in Fig. 2). The viscoelastic moduli were found to be insensitive to the oscillation frequency for all materials at 80 °C within our experimental window (0.1 to 100 rad s^{-1}). For all tests at 80 °C, the value of $\tan(\delta) = G''/G'$ in the linear plateau region was between 0.02 and 0.1 and G'' is omitted from plots for clarity. From this LAOS test, the first-harmonic storage modulus G_1'[74] was fit to a constant value in the small amplitude plateau region to obtain the linear viscoelastic storage modulus G'_{LVE} (referred to as the hot gel elastic storage modulus); any higher harmonic responses are neglected. Apparent failure manifested as extreme non-linearity; we emphasize the apparent nature of this failure stress, σ_Y^*, and that it may not be a true material property since the failure may include both the cohesive failure (due to sample yield) and the adhesive failure (due to boundary slip). Despite the approximate nature of the failure stress, we report it here as it indicates the limits of the available data and is still representative of the observed mechanical failure.

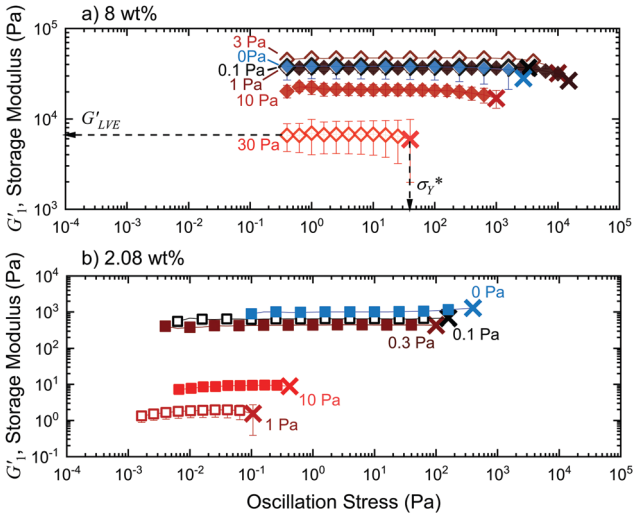

Fig. 5 Softer and weaker gels result when formed under applied unidirectional shear stress. Oscillatory shear-stress amplitude sweeps at 3 rad s^{-1} of formed hot gels at 80 °C for (a) 8 wt% and (b) 2.08 wt%, for a range of applied stress during gelation (0–30 Pa, as labeled). Data sets truncated at apparent failure stress indicated by × symbols. In regions of overlapping data, point density is decreased for readability. Error bars are from repeat experiments. The sub-dominant G''_1 data are omitted for clarity. Color and shape of symbols for a given sample are consistent across all dynamic gelation figures.

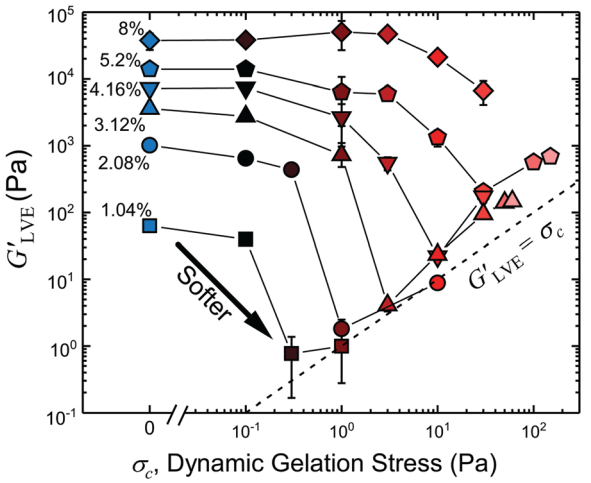

Fig. 6 Summary of hot gel storage modulus at 80 °C as a function of concentration and stress applied during gelation: (c, σ_c). Blue data shown at 0 Pa from true quiescent gelation (not SAOS). Dashed line shows $G'_{LVE} = \sigma_c$, as a comparative reference for a peculiar observation with data at the highest dynamic gelation stresses. Color and shape of symbols for a given sample are consistent across all dynamic gelation figures.

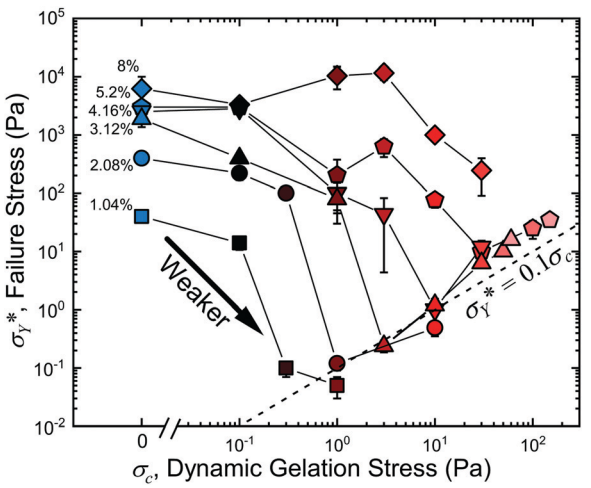

Fig. 7 Apparent failure stress σ^*_Y, for all concentrations at 80 °C as a function of the applied stress during gelation. Dashed line shows $\sigma^*_Y = 0.1\sigma_c$, another peculiar observation with data at the highest dynamic gelation stresses. Color and shape of symbols for a given sample are consistent across all dynamic gelation figures.

Fig. 5 shows the elastic storage modulus, G'_1, for MC at 8 wt% and 2.08 wt% gelled under increasing stresses (similar data for all other compositions in Fig. S11–S14, ESI.†). The MC material in this study does not display strain stiffening behavior in LAOS, in contrast to other types of MC.[29,36] For 8 wt%, across two-and-a-half decades of applied flow stress σ_c, the resulting hot gel storage modulus decreases by an order of magnitude (the gel is much less stiff), and the apparent failure stress decreases by over an order of magnitude (the gel breaks much more easily). For 2.08 wt%, the change of storage modulus and apparent failure stress with the applied stress is not monotonic. Both the modulus and failure stress continue to decrease with the applied stress until $\sigma_c = 1$ Pa, when the applied stress is large enough to break the network entirely. No gel forms while this stress is applied (see Fig. 4c), and a soft viscoelastic solid forms after the stress is removed. For such viscoelastic solids, when the applied stress is further increased, the modulus and failure stress increase unexpectedly, though they remain much lower than the quiescent hot gel values.

The results of Fig. 5 and similar results in Fig. S11–S14 (ESI†) for other concentrations are summarized in Fig. 6 (linear storage modulus, G'_{LVE}) and Fig. 7 (failure stress, σ^*_Y,). All measured MC concentrations less than 8 wt% show a non-monotonic trend where the sharp decrease in G'_{LVE} is followed by a gradual increase as the dynamic gelation stress increases. At very low gelation stresses (0.1 Pa), G'_{LVE} is within experimental variation of the true quiescent values, and at higher stresses, G'_{LVE} decreases below the true quiescent modulus. At even higher applied stresses, gelation is entirely prohibited and solid gel behavior is only apparent after stress removal. In this stress range, increasing the applied stress causes a comparatively stiffer and stronger gel to ultimately form. In a peculiar observation which may be coincidental, this gradual increase follows approximately along the line of $G'_{LVE} = \sigma_c$, suggesting the hot gel moduli in this regime have become insensitive to MC concentration and instead depends more on the applied dynamic gelation stress. A consequence of G'_{LVE} scaling with σ_c is that it indicates a constraint on the processing–structure–properties design space of the hot gel; the minimum achievable G'_{LVE} is approximately equal to the applied stress when gelation is just inhibited.

The trends for σ_Y^*, in Fig. 7 are not as clear as for G'_{LVE}, yet the same overall trends are observed. We observe a decrease followed by a concentration-insensitive increase for samples below 8 wt%. Above the concentration-dependent critical stress, materials appear to approximately follow the line of $\sigma_Y^* = 0.1\sigma_c$. Similar to the storage modulus, G'_{LVE}, the scaling of σ_Y^* with σ_c constrains the minimum σ_Y^*, obtainable through dynamic gelation with an applied stress where gelation is just inhibited.

There are major practical implications for this huge range of resulting mechanical properties. In the example of a gelling film on a vertical surface, a 1 mm thick layer results in a stress at the substrate of approximately 10 Pa (see ESI,† Section I and Fig. 2b). For a concentration such as 2.08 wt%, this means that rather than being able to support a load of 600 Pa (true quiescent failure stress able to affix the gel on the surface), the film coating might be expected to fail at a loading of less than 1 Pa and slump down, leaving only a thin layer behind.

3.3. Inferring microstructure from rheology

The dramatic changes in mechanical properties suggest significant microstructural differences among materials gelled quiescently and those gelled under unidirectional applied stress conditions. We conjecture that the difference is caused by fewer crosslinks and thus an increased distance between crosslinks in the MC gel, as the applied stress suppresses the crosslink formation during the gelation and the average distance between crosslinks is increased. This results in an overall sparser connectivity and consequently, a softer and weaker material compared to the quiescent gelation case. To quantify such structural features of the MC gel, in this section we examine the validity of a semi-solid filament-based model for our data and estimate the distance between crosslinks, l_c, using our rheological measurements of the linear elastic modulus, G'_{LVE}, and the apparent failure stress, σ_Y^*.

For the quiescently formed gels, their linear viscoelastic moduli increase with concentration, as expected. Fig. 8a shows the linear elastic modulus of the quiescent gels *versus* concentration, and the solid line indicates a power law fit of 2.4 ± 0.2. The concentration, c, is calculated from the weight fraction, assuming a density of 1.39 g mL^{-1} for the polymer and additive volume. This scaling is consistent with the semiflexible polymer filament-based network model, developed by McKintosh *et al.*,[62] which predicts the scaling of $G_0 \sim c^{5/2}$. Here, we assume $G'_{LVE} = G_0$, since G'' is negligible. This model was originally developed to describe the elasticity of semiflexible polymer networks and has been applied to large molecular weight MC gels recently.[29] The semi-flexibility assumption of the model requires that the mesh size, ξ, and the crosslink distance, l_c, are smaller than the persistence length, l_p, of the fibril. According to the model, the elastic modulus, G_0, is related to the persistence length, l_p, and the distance between crosslinks, l_c, as[63]

$$G_0 = 6\rho k_B T \frac{l_p^2}{l_c^3}, \quad (1)$$

where k_B is the Boltzmann constant; T is temperature. ρ is the fibril density (length per volume), which is related to the volume fraction of polymer, ϕ_P, and the fibril radius, r, by $\rho = \phi_P/x\pi r^2$; where x is the volume fraction of polymer within the fibril. The elastic stress comes from the bending and stretching of polymer strands between crosslinks. Compared with the modulus for rubber-like polymer networks,[75,76] $G_0 \sim \nu k_B T \sim \frac{\rho}{l_c} k_B T$, where the polymer strands are flexible and act as random coils, the elasticity of semiflexible polymer networks is multiplied by a factor of $\left(\frac{l_p}{l_c}\right)^2$, which is larger than one to be self-consistent with modeling assumptions. MC fibrils are reported to have a persistence length of approximately 30 nm and contain 40% polymer by volume; the fibril radius is 7.5 nm, which is constant regardless of MC concentration and molecular weight within a certain range.[29] Using these quantities and eqn (1), the distance between crosslinks, l_c, for the quiescent

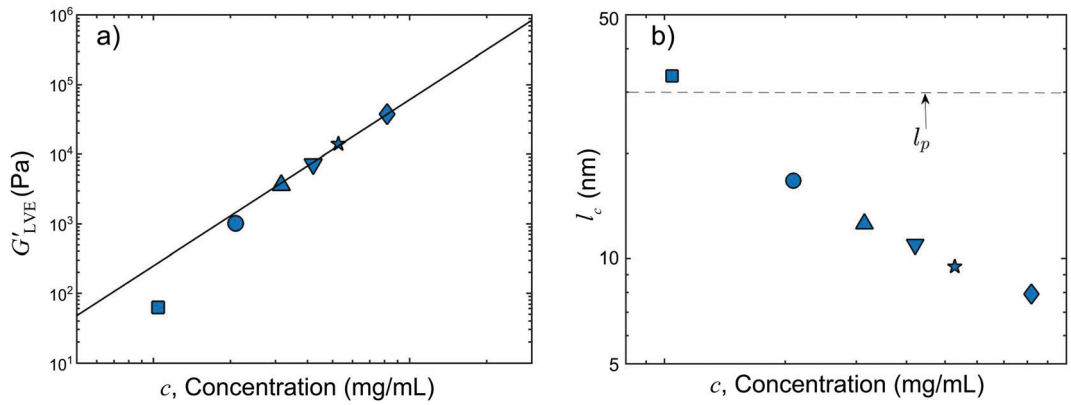

Fig. 8 The validity of the semiflexible chain network theory for METHOCEL™ A15 MC gel across the concentrations studied: (a) linear storage modulus, G'_{LVE}, at 3 rad s^{-1}, 80 °C, *versus* polymer concentration, c. The solid line is the power law fit to the data, which gives the scaling of 2.4 ± 0.2. (b) The distance between crosslinks, l_c, for quiescent gels, is smaller than the persistence length, l_p, for most concentrations. l_c is calculated from G'_{LVE} by assuming the radius of fibril, r, being 7.5 nm and l_p being 30 nm.[29] The dashed line represents the persistence length, l_p, which is higher than l_c except for the lowest concentration.

gels is calculated from the measured elastic modulus, G'_{LVE}, as shown in Fig. 8b. With the increase of polymer concentration, a more densely crosslinked gel is formed and the distance between crosslinks decreases. For all concentrations except the lowest one (1.04 wt%), l_c is lower than l_p, suggesting this METHOCEL™ A15 MC forms a semiflexible polymer network[62] and the model by McKintosh is applicable for studied concentrations higher than 1.04 wt%. The l_c for the gel with the lowest concentration (1.04 wt%) is slightly larger than l_p, suggesting a gel network with sparser crosslinking and more flexible polymer strands between crosslinks that gives rise to a softer gel. This is consistent with the modulus at 1.04 wt% being lower than the fit line in in Fig. 8a. It should be noted that the values of persistence length, fibril radius, and other quantities mentioned above have only been validated for the specific MC gels studied by McAllister *et al.*[29,36] (larger molecular weight than is studied here), so the calculated l_c in Fig. 8b may only be qualitatively correct. For any other calculations in this paper, we have not used those values.

For inferring the structure of the dynamically formed gels, we assume that applying stress during gelation increases the distance between crosslinks, changing the crosslink density of the gel by disrupting their formation, but the fibril persistence length and dimensions are unaffected. Within this strict assumption, the effect on the structure can be quantified by calculating the relative average crosslink distance, l_{cd}/l_c, defined as the ratio of the average distance between crosslinks of the dynamic gel divided by the crosslink distance of the quiescent gel of the same concentration. From eqn (1) we can see that for each concentration, the relative average crosslink distance can be determined by $\frac{l_{cd}(\sigma_c)}{l_c} = \left(\frac{G'_{LVE}}{G'_{LVE}(\sigma_c)}\right)^{1/3}$, and the results are shown in Fig. 9. For each concentration, the relative average crosslink distance initially increases with the applied stress as crosslink formation during gelation is disrupted. Above the concentration-dependent critical applied stresses, when the gels are unable to fully form until the stress is removed, the relative distance decreases, but remains larger than one; this suggests that the crosslink density is always less than the quiescent gel. A possible caveat to this is that as the distance between crosslinks increases, the semiflexible condition is no longer satisfied and the model loses accuracy. In this case, a softer and more flexible gel network may be formed.

The semiflexible polymer network model also predicts a critical stiffening stress, σ_{cs}, above which a gel stiffens,[77,78]

$$\sigma_{cs} = \rho k_B T \frac{l_p}{l_c^2}. \quad (2)$$

In principle, the bending rigidity, $\kappa = k_B T l_p$, is a constant for different networks composed of the same type of fibril and at the same temperature. This has been applied to successfully predict the critical stress at which some MC gels undergo strain stiffening in LAOS.[29] Although we do not observe strain stiffening for our MC gels, we hypothesize that this same critical stress is associated with nonlinearity and a rapid change of the mechanical response which may cause mechanical failure of the network. By combining eqn (1) and (2), we obtain $\sigma_{cs} = \left(\frac{1}{6}\right)^{2/3}\left(\frac{k_B T}{l_p}\right)^{1/3}\left(\sqrt{\rho}G_0\right)^{2/3}$. The fibril density, ρ, is proportional to the concentration, c, if we assume a constant fibril radius, r. Therefore, the model predicts a critical stress scaling $\sigma_{cs} \sim \left(\sqrt{c}G_0\right)^{2/3}$ for a constant persistence length, l_p.[63] Fig. 10 shows the apparent failure stress, σ^*_Y, as a function of $\sqrt{c}G'_{LVE}$ to assess the prediction of $\sigma_{cs} \sim \left(\sqrt{c}G_0\right)^{2/3}$. For quiescently formed gels, which are shown in blue, the power law scaling of σ^*_Y, to $\sqrt{c}G'_{LVE}$ is 0.7 ± 0.2, shown as a solid blue line. This range is consistent with

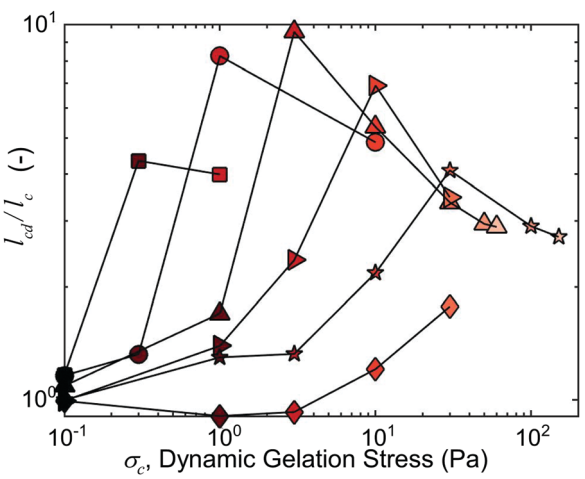

Fig. 9 The effect of applied stress, σ_c, on the apparent crosslink distance inferred from the model of eqn (1): the average distance between crosslinks of dynamic gel, l_{cd}, normalized by that of the quiescent gel, l_c, of the same concentration as a function of applied stress. Symbols indicate different material concentrations and are consistent with the representation in Fig. 8 and 10.

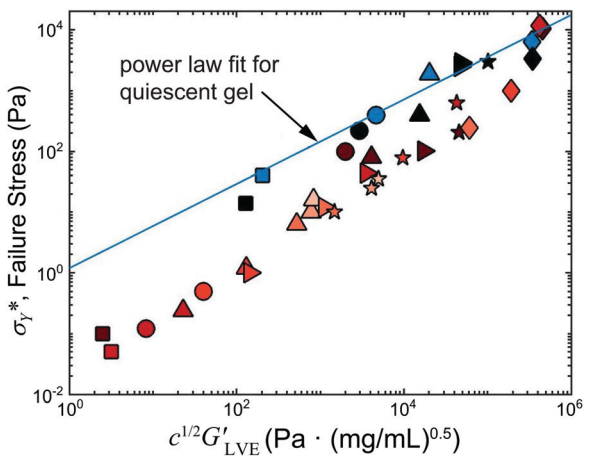

Fig. 10 The dependence of σ^*_Y on $\sqrt{c}G'_{LVE}$ for both quiescent and dynamic gels, which is more sensitive for the dynamic gel than the quiescent gel. The gel fails before stiffening can be observed. The solid blue line is the best fit for the quiescent gel, which gives the scaling of 0.7 ± 0.2, consistent with the model prediction. The failure stresses of dynamic gels are lower than the quiescent gel fit. Symbols indicate concentration, colors indicate applied stress (same meaning as in prior figures).

the critical stiffening stress scaling predicted by the model. This suggests that the critical stiffening stress prediction is meaningful for failure behavior, even if stiffening is not observed. For dynamic gels, the scaling of critical stiffening stress predicted by the model is no longer applicable, and the failure stress is lower than the quiescent gel fit, suggesting a different structure is being formed than assumed by the model. The lower failure stress also suggests that by applying stress during gelation, the ultimate mode of failure of MC gels changes from fracture to yielding and the failure stress is greatly reduced. In this case, the failure stress is lower than the critical stiffening stress, and the MC gel fails before it stiffens. Although the failure stress is lower, there is still a proportionality between σ_Y^*, and $\sqrt{c}G'_{LVE}$. The scaling appears close to 2/3 for lower values of G'_{LVE} at a given concentration, but is much more sensitive at higher values of G'_{LVE}.

By comparing both linear (elastic modulus, G'_{LVE}) and non-linear (apparent failure stress, σ_Y^*,) rheology with the filament-based network model, we have shown that this model is applicable for the quiescently formed MC gels at this molecular weight, even though no strain stiffening is observed in LAOS. However, for gels formed under unidirectional stress, the crosslink formation is disrupted and the model is less credible, suggesting that a fundamentally different structure is formed.

Additionally, we infer the effect of the applied stress on the structural features of the MC fibrillar network by using a filament-based mechanical model. By comparing the linear elasticity scaling and the inferred crosslink distances, we show that the semiflexible filament-based mechanical model is applicable to our quiescently formed gels, even though they are lower molecular weight than prior studies and do not show strain stiffening in LAOS. For dynamically formed gels, the distance between crosslinks appears to increase with applied stress, leading to a softer and easier to break hot gel. The dynamically formed gels undergo apparent yielding rather than the strain stiffening predicted by the mechanical model.

Here we only characterize hot gel properties in the same direction as the applied stress (*i.e.* the rotational direction). It is possible that MC fibrils may form an anisotropic aligned structure under the unidirectional applied stress. If so, it is likely that properties such as stiffness, failure stress, diffusivity, *etc.*, may be anisotropic and characterization of such anisotropic properties would serve as interesting future studies, including rheological, structural, and transport properties through MC networks. Outside the scope of this paper is the direct characterization of the molecular-level structures of the gel under shear flows, which would require the development of microscopy protocols that combine controlled stress conditions and high temperatures.

The results presented here demonstrate that small stresses applied during gelation can have a significant effect on the gel temperature, the structure, and consequently, the mechanical properties of the hot gel, such as the linear viscoelasticity and the failure stress. The results are important for MC materials but also have implications for the vast array of gelling soft materials which—whether acknowledged or not—often undergo gelation at small non-zero stress conditions that may suppress structure formation and change the resulting gel point and gelled properties. This may be catastrophic for some applications, but also opens possibilities for engineering material structure and properties by using low-stress-amplitude processing in non-equilibrium conditions.

4. Conclusions

We applied constant unidirectional shear stresses during the gelation of aqueous methylcellulose to obtain rheological properties in both the liquid and hot gel states across a wide range of MC concentrations and dynamic stresses. Applying stress was found to make gelation more difficult (*i.e.* gel temperature increased) or inhibit gelation entirely until removal of the applied load. Significantly softer and weaker gels were formed under dynamic conditions, with lower concentrations showing non-monotonic dependence of properties on σ_c. For low concentration solutions, gelation appears to be inhibited entirely above a critical stress, and the gel forms only after the stress is removed. Given the sensitivity of gel temperatures of some concentrations to a relatively small unidirectional stress (*e.g.* for 2.08 wt%, G'_{LVE} decreasing by over two orders of magnitude at σ_c = 1 Pa), the stress-dependent gel temperature raises questions for any gelation test performed at finite stress magnitude, including SAOS. Clearly, if one's application relies on gelation occurring at a particular temperature, an unaccounted-for delay or inhibition of this process could have unfavorable implications. Yet this phenomenon could also allow for more design freedom in the available material properties and rheology. For example, if one does not want a material to form a rigid gel in a hot environment, applying a flow stress could inhibit gelation or significantly change the resulting properties. This is not limited to materials that exhibit a "gel temperature" and can also be applied to materials where flow may affect structure formation including the restructuring of thixotropic materials.

Conflicts of interest

There are no conflicts to declare.

Acknowledgements

This work was supported by Corporate R&D at The Dow Chemical Company. We acknowledge the support of Keith Harris. Since the completion of this grant, the Pharma Solutions business of Dow, to which this work was aligned, has moved to International Flavors & Fragrances (IFF). References in the text (such as author affiliations) to the former portion of Dow that is now part of IFF are referred to as IFF, while those that remain with Dow are mentioned with the Dow name.

References

1 E. Touitou and M. Donbrow, Influence of additives on (hydroxyethyl) methylcellulose properties: relation between gelation temperature change, compressed matrix integrity and drug release profile, *Int. J. Pharm.*, 1982, **11**(2), 131–148.

2 K. Mitchell, J. L. Ford, D. J. Armstrong, P. N. C. Elliott, C. Rostron and J. E. Hogan, The influence of concentration on the release of drugs from gels and matrices containing Methocel, *Int. J. Pharm.*, 1993, **100**, 155–163.

3 V. R. Babu, M. Sairam, K. M. Hosamani and T. M. Aminabhavi, Preparation of sodium alginate-methylcellulose blend microspheres for controlled release of nifedipine, *Carbohydr. Polym.*, 2007, **69**(2), 241–250.

4 L.-H. Chen and P. S. Doyle, Design and use of a thermogelling methylcellulose nanoemulsion to formulate nanocrystalline oral dosage forms, *Adv. Mater.*, 2021, **33**(29), 2008618.

5 D. A. Bell, Methylcellulose as a structure enhancer in bread baking, *Cereal Foods World*, 1990, **35**, 1001–1006.

6 T. Sanz, A. Salvador, G. Vélez, J. Muñoz and S. M. Fiszman, Influence of ingredients on the thermo-rheological behaviour of batters containing methylcellulose, *Food Hydrocoll.*, 2005, **19**(5), 869–877.

7 J. Bousquières, C. Michon and C. Bonazzi, Functional properties of cellulose derivatives to tailor a model sponge cake using rheology and cellular structure analysis, *Food Hydrocoll.*, 2017, **70**, 304–312.

8 F. K. Akthar and J. R. G. Evans, High porosity (>90%) cementitious foams, *Cem. Concr. Res.*, 2010, **40**(2), 352–358.

9 M. R. Du, H. W. Jing, W. H. Duan, G. S. Han and S. J. Chen, Methylcellulose stabilized multi-walled carbon nanotubes dispersion for sustainable cement composites, *Constr. Build. Mater.*, 2017, **146**(15), 76–85.

10 M.-C. Chen, G. H.-C. Yen and B.-H. Chiang, Antimicrobial and physicochemical properties of methylcellulose and chitosan films containing a preservative, *J. Food Process. Preserv.*, 1996, **20**(5), 379–390.

11 A. Pinotti, M. A. García, M. N. Martino and N. E. Zaritzky, Study on microstructure and physical properties of composite films based on chitosan and methylcellulose, *Food Hydrocoll.*, 2007, **21**(1), 66–72.

12 M. A. Mingsukang, M. H. Buraidah, M. A. Careem, I. Albinsson, B. E. Mellander and A. K. Arof, Investigation of counter electrode materials for gel polymer electrolyte based quantum dot sensitized solar cells, *Electrochim. Acta*, 2017, **241**, 487–496.

13 B. C. Church, T. H. Sanders, R. F. Speyer and J. K. Cochran, Thermal expansion matching and oxidation resistance of Fe–Ni–Cr interconnect alloys, *Mater. Sci. Eng., A*, 2007, **452–453**(15), 334–340.

14 J. Pusz, A. Smirnova, A. Mohammadi and N. M. Sammes, Fracture strength of micro-tubular solid oxide fuel cell anode in redox cycling experiments, *J. Power Sources*, 2007, **163**(2), 900–906.

15 D. K. Bhui, S. Pyne, P. Sarkar, H. Bar, G. P. Sahoo and A. Misra, Temperature controlled synthesis of silver nanostructures of variable morphologies in aqueous methyl cellulose matrix, *J. Mol. Liq.*, 2011, **158**(3), 170–174.

16 D. K. Bhui and A. Misra, Synthesis of worm like silver nanoparticles in methyl cellulose polymeric matrix and its catalytic activity, *Carbohydr. Polym.*, 2012, **89**(3), 830–835.

17 M. Ogawa, R. T. Parmley, H. L. Bank and S. S. Spicer, Human marrow erythropoiesis in culture. I. characterization of methylcellulose colony assay, *Blood*, 1976, **48**(3), 407–417.

18 S. Goldblum, Y. K. Bae, W. F. Hink and J. Chalmers, Protective effect of methylcellulose and other polymers on insect cells subjected to laminar shear stress, *Biotechnol. Prog.*, 1990, **6**(5), 383–390.

19 L. Yang, M. H. Soonpaa, E. D. Adler, T. K. Roepke, S. J. Kattman, M. Kennedy, E. Henckaerts, K. Bonham, G. W. Abbott, R. M. Linden, L. J. Field and G. M. Keller, Human cardiovascular progenitor cells develop from a KDR+ embryonic-stem-cell-derived population, *Nature*, 2008, **453**(7194), 524–528.

20 T. Kato, M. Yokoyama and A. Takahashi, Melting temperatures of thermally reversible gels IV. methyl cellulose-water gels, *Colloid Polym. Sci.*, 1978, **256**, 15–21.

21 N. Sarkar, Thermal gelation properties of methyl and hydroxypropyl methylcellulose, *J. Appl. Polym. Sci.*, 1979, **24**(4), 1073–1087.

22 A. Haque and E. R. Morris, Thermogelation of methylcellulose. Part I: molecular structures and processes, *Carbohydr. Polym.*, 1993, **22**(3), 161–173.

23 C. Clasen and W.-M. Kulicke, Determination of viscoelastic and rheo-optical material functions of water-soluble cellulose derivatives, *Prog. Polym. Sci.*, 2001, **26**, 1839–1919.

24 T. Chatterjee, A. I. Nakatani, R. Adden, M. Brackhagen, D. Redwine, H. Shen, Y. Li, T. Wilson and R. L. Sammler, ''Structure and properties of aqueous methylcellulose gels by small-angle neutron scattering, *Biomacromolecules*, 2012, **13**(10), 3355–3369.

25 J. P. A. Fairclough, H. Yu, O. Kelly, A. J. Ryan, R. L. Sammler and M. Radler, Interplay between gelation and phase separation in aqueous solutions of methylcellulose and hydroxypropylmethylcellulose, *Langmuir*, 2012, **28**, 10551–10557.

26 S. A. Arvidson, J. R. Lott, J. W. McAllister, J. Zhang, F. S. Bates, T. P. Lodge, R. L. Sammler, Y. Li and M. Brackhagen, Interplay of phase separation and thermoreversible gelation in aqueous methylcellulose solutions, *Macromolecules*, 2013, **46**(1), 300–309.

27 J. R. Lott, J. W. McAllister, S. A. Arvidson, F. S. Bates and T. P. Lodge, Fibrillar structure of methylcellulose hydrogels, *Biomacromolecules*, 2013, **14**(8), 2484–2488.

28 J. R. Lott, J. W. McAllister, M. Wasbrough, R. L. Sammler, F. S. Bates and T. P. Lodge, Fibrillar structure in aqueous methylcellulose solutions and gels, *Macromolecules*, 2013, **46**(24), 9760–9771.

29 J. W. McAllister, J. R. Lott, P. W. Schmidt, R. L. Sammler, F. S. Bates and T. P. Lodge, Linear and nonlinear rheological behavior of fibrillar methylcellulose hydrogels, *ACS Macro Lett.*, 2015, **4**(5), 538–542.

30 A. E. Metaxas, M. L. Coughlin, C. K. Hansen, F. S. Bates, T. P. Lodge and C. S. Dutcher, Microfluidic filament thinning of aqueous, fibrillar methylcellulose solutions, *Phys. Rev. Fluids*, 2020, **5**, 113302.
31 B. L. Micklavzina, A. E. Metaxas and C. S. Dutcher, Microfluidic rheology of methylcellulose solutions in hyperbolic contractions and the effect of salt in shear and extensional flows, *Soft Matter*, 2020, **16**, 5273.
32 M. L. Coughlin, L. Liberman, S. P. Ertem, J. Edmund, F. S. Bates and T. P. Lodge, Methyl cellulose solutions and gels: fibril formation and gelation properties, *Prog. Polym. Sci.*, 2021, **112**, 101324.
33 R. Bayer and M. Knarr, Thermal precipitation or gelling behaviour of dissolved methylcellulose (MC) derivatives-behaviour in water and influence on the extrusion of ceramic pastes. Part 1: fundamentals of MC-derivatives, *J. Eur. Ceram. Soc.*, 2012, **32**(5), 1007–1018.
34 K. Kobayashi, C. Huang and T. P. Lodge, Thermoreversible gelation of aqueous methylcellulose solutions, *Macromolecules*, 1999, **32**(21), 7070–7077.
35 N. Isobe and S. Shimizu, Salt-induced LCST-type thermal gelation of methylcellulose: quantifying non-specific interactions via fluctuation theory, *Phys. Chem. Chem. Phys.*, 2020, **22**, 15999–16006.
36 J. W. McAllister, P. W. Schmidt, K. D. Dorfman, T. P. Lodge and F. S. Bates, Thermodynamics of aqueous methylcellulose solutions, *Macromolecules*, 2015, **48**(19), 7205–7215.
37 V. V. Ginzburg, R. L. Sammler, W. Huang and R. G. Larson, Anisotropic self-assembly and gelation in aqueous methylcellulose-theory and modeling, *J. Polym. Sci., Part B: Polym. Phys.*, 2016, **54**(16), 1624–1636.
38 A. Z. Nelson, K. S. Schweizer, B. M. Rauzan, R. G. Nuzzo, J. Vermant and R. H. Ewoldt, Designing and transforming yield-stress fluids, *Curr. Opin. Solid State Mater. Sci.*, 2009, **23**(5), 100758.
39 S. M. Tosh and G. Marangoni, Determination of the maximum gelation temperature in gelatin gels, *Appl. Phys. Lett.*, 2004, **84**, 4242–4244.
40 C. Li, Q. Han, Y. Guan and Y. Zhang, Thermal gelation of chitosan in an aqueous alkali-urea solution, *Soft Matter*, 2014, **10**, 8245–8253.
41 H.-L. Yi and C.-C. Hua, PBTTT-C16 sol-gel transition by hierarchical colloidal bridging, *Soft Matter*, 2018, **14**, 1270–1280.
42 X. T. Le and S. L. Turgeon, Rheological and structural study of electrostatic cross-linked xanthan gum hydrogels induced by b-lactoglobulin, *Soft Matter*, 2013, **9**, 3063–3073.
43 Y. Zhao, K. Paso, L. Kumar, J. Safieva, M. Z. B. Sariman and J. Sjoblom, Controlled shear stress and controlled shear rate nonoscillatory rheological methodologies for gelation point determination, *Energy Fuels*, 2013, **27**, 2025–2032.
44 S. Da Pieve, S. Calligaris, E. Co, M. C. Nicoli and A. G. Marangoni, Shear nanostructuring of monoglyceride organogels, *Food Biophys.*, 2010, **5**, 211–217.
45 M. Chopin-Doroteo, J. A. Morales-Rueda, E. Dibildox-Alvarado, M. A. Charó-Alonso, A. D. L. Peña-Gil and J. F. Toro-Vazquez, The effect of shearing in the thermomechanical properties of candelilla wax and candelilla wax-tripalmitin organogels, *Food Biophys.*, 2011, **6**, 359–376.
46 F. M. Alvarez-Mitre, J. A. Morales-Rueda, E. Dibildox-Alvarado, M. A. Charó-Alonso and J. F. Toro-Vazquez, Shearing as a variable to engineer the rheology of candelilla wax organogels, *Food Res. Int.*, 2012, **49**, 580–587.
47 F. R. Lupi, D. Gabriele, D. Facciolo, N. Baldino, L. Seta and B. de Cindio, Effect of organogelator and fat source on rheological properties of olive oil-based organogels, *Food Res. Int.*, 2012, **46**, 177–184.
48 A. Omari, G. Chauveteau and R. Tabary, Gelation of polymer solutions under shear flow, *Colloids Surf., A*, 2002, **225**, 37–48.
49 S. Lazzari, G. M. Maggioni, M. Soos, H. Wu and M. Morbidelli, Shear-stability and gelation of inverse latexes, *Soft Matter*, 2013, **9**, 10866–10876.
50 M. Kane, M. Djabourov and J.-L. Volle, Rheology and structure of waxy crude oils in quiescent and under shearing conditions, *Fuel*, 2004, **83**, 1591–1605.
51 W. Carvalho and M. Djabourov, Physical gelation under shear for gelatin gel, *Rheol. Acta*, 1997, **36**, 591–609.
52 N. Badiei, A. M. Sowedan, D. J. Curtis, M. R. Brown, M. J. Lawrence, A. I. Campbell, A. Sabra, P. A. Evans, J. W. Weisel, I. N. Chernysh, C. Nagaswami, P. R. Williams and K. Hawkins, Effects of unidirectional flow shear stresses on the formation, fractal microstructure and rigidity of incipient whole blood clots and fibrin gels, *Clin. Hemorheol. Microcirc.*, 2015, **60**(4), 451–464.
53 R. E. Corman and R. H. Ewoldt, Mapping linear viscoelasticity for design and tactile intuition, *Appl. Rheol.*, 2019, **29**(1), 141–161.
54 R. H. Ewoldt and G. H. McKinley, Mapping thixo-elasto-visco-plastic behavior, *Rheol. Acta*, 2017, **56**(3), 195–210.
55 M. Knarr and R. Bayer, The shear dependence of the methylcellulose gelation phenomena in aqueous solution and in ceramic paste, *Carbohydr. Polym.*, 2014, **111**, 80–88.
56 P. W. Schmidt, S. Morozova, S. P. Ertem, M. L. Coughlin, I. Davidovich, Y. Talmon, T. M. Reineke, F. S. Bates and T. P. Lodge, Internal structure of methylcellulose fibrils, *Macromolecules*, 2020, **53**, 398–405.
57 G. Colombo, S. Kim, T. Schweizer, B. Schroyen, C. Clasen, J. Mewis and J. Vermant, Superposition rheology and anisotropy in rheological properties of sheared colloidal gels, *J. Rheol.*, 2017, **61**, 1035–1048.
58 G. G. Fuller, *Optical Rheometry of Complex Fluids*, Oxford University Press, New York, 1995.
59 A. P. R. Eberle and L. Porcar, Flow-SANS and rheo-SANS applied to soft matter, *Curr. Opin. Colloid Interface Sci.*, 2012, **17**(1), 33–43.
60 S. K. Dutta, A. Mbi, R. C. Arevalo and D. L. Blair, Development of a confocal rheometer for soft and biological materials, *Rev. Sci. Instrum.*, 2013, **84**, 063702.
61 G. Colombo, R. Massaro, S. Coleman, J. Läuger, P. V. Puyvelde and J. Vermant, Ultrafast imaging of soft materials during shear flow, *Korea-Aust. Rheol. J.*, 2019, **31**(4), 229–240.

62 F. C. MacKintosh, J. Käs and P. A. Janmey, Elasticity of semiflexible biopolymer networks, *Phys. Rev. Lett.*, 1995, **75**, 4425–4428.
63 N. Y. Yao, C. P. Broedersz, Y.-C. Lin, K. E. Kasza, F. C. MacKintosh and D. A. Weitz, Elasticity in ionically cross-linked neurofilament networks, *Biophys. J.*, 2010, **98**(10), 2147–2153.
64 Y. Li, H. Shen, J. W. Lyons, R. L. Sammler, M. Brackhagen and D. M. Meunier, Size-exclusion chromatography of ultrahigh molecular weight methylcellulose ethers and hydroxypropyl methylcellulose ethers for reliable molecular weight distribution characterization, *Carbohydr. Polym.*, 2016, **138**, 290–300.
65 United States Pharmacopoeial Convention, *The United States Pharmacopoeia: The National Formulary*, United Book Press, Inc, Baltimore, MD, 2012.
66 H. H. Winter and F. Chambon, Analysis of linear viscoelasticity of a crosslinking polymer at the gel point, *J. Rheol.*, 1986, **30**, 367–382.
67 F. Chambon and H. H. Winter, Linear viscoelasticity at the gel point of a crosslinking PDMS with imbalanced stoichiometry, *J. Rheol.*, 1987, **31**, 683–697.
68 J. Desbrières, M. Hirrien and S. B. Ross-Murphy, Thermogelation of methylcellulose: rheological considerations, *Polymer*, 2000, **41**, 2451–2461.
69 R. H. Ewoldt, M. T. Johnston and L. M. Caretta, Experimental challenges of shear rheology: how to avoid bad data, in *Complex Fluids in Biological Systems*, ed. S. E. Spagnolie, Springer, 2015.
70 C. W. Macosko, *Rheology: Principles, Measurements, and Applications*, Wiley, New York, 1994.
71 B. Stoeber, Z. Yang, D. Liepmann and S. J. Muller, Flow control in microdevices using thermally responsive triblock copolymers, *J. Microelectromech. Syst.*, 2005, **14**, 207–213.
72 N. Sarkar, *Carbohydr. Polym.*, 1995, **26**, 195–203.
73 E. M. Furst and T. M. Squires, *Microrheology*, Oxford University Press, 2018.
74 R. H. Ewoldt, Defining nonlinear rheological material functions for oscillatory shear, *J. Rheol.*, 2013, **57**, 177–195.
75 W. W. Graessley, *Polymeric liquids and networks: structure and properties*, Garland Science, New York and London, 2003.
76 M. Rubinstein and R. H. Colby, *Polymer physics*, Oxford University Press, New York, 2013.
77 M. L. Gardel, J. H. Shin, F. C. MacKintosh, L. Mahadevan, P. A. Matsudaira and D. A. Weitz, Scaling of F-Actin network rheology to probe single filament elasticity and dynamics, *Phy. Rev. Lett.*, 2004, **93**(18), 188102.
78 M. L. Gardel, J. H. Shin, F. C. MacKintosh, L. Mahadevan, P. Matsudaira and D. A. Weitz, Elastic behavior of cross-linked and bundled actin networks, *Science*, 2014, **304**(28), 1301–1305.